



**HAL**  
open science

# Exploring the dynamics of passive isolation flap valves in dust explosion mitigation: a model-based approach and its implications

Yann Grégoire, Emmanuel Leprette, Christophe Proust

## ► To cite this version:

Yann Grégoire, Emmanuel Leprette, Christophe Proust. Exploring the dynamics of passive isolation flap valves in dust explosion mitigation: a model-based approach and its implications. *Process Safety and Environmental Protection*, 2024, 184, pp.284-299. 10.1016/j.psep.2024.02.003 . ineris-04492477

**HAL Id: ineris-04492477**

**<https://ineris.hal.science/ineris-04492477>**

Submitted on 6 Mar 2024

**HAL** is a multi-disciplinary open access archive for the deposit and dissemination of scientific research documents, whether they are published or not. The documents may come from teaching and research institutions in France or abroad, or from public or private research centers.

L'archive ouverte pluridisciplinaire **HAL**, est destinée au dépôt et à la diffusion de documents scientifiques de niveau recherche, publiés ou non, émanant des établissements d'enseignement et de recherche français ou étrangers, des laboratoires publics ou privés.



Contents lists available at ScienceDirect

# Process Safety and Environmental Protection

journal homepage: [www.journals.elsevier.com/process-safety-and-environmental-protection](http://www.journals.elsevier.com/process-safety-and-environmental-protection)

## Exploring the dynamics of passive isolation flap valves in dust explosion mitigation: a model-based approach and its implications

Yann Grégoire<sup>a,\*</sup>, Emmanuel Leprette<sup>a</sup>, Christophe Proust<sup>a,b</sup><sup>a</sup> Institut National de l'Environnement Industriel et des Risques, PARC ALATA, BP2, Verneuil-en-Halatte 60550, France<sup>b</sup> Sorbonne Universities, Technological Univ. of Compiègne, ESCOM, TIMR Centre Pierre Guillaumat, Compiègne 60200, France

### ARTICLE INFO

#### Keywords:

Dust explosions  
Explosion isolation  
Explosion mitigation  
Explosion modelling

### ABSTRACT

Passive isolation flap valves are relatively simple devices widely used in the process industries. However, as with any explosion mitigation technique, they work only within well-defined conditions, and the underlying physics makes any prediction difficult. The current paper presents new methods and findings, which rely on experiments on passive flap valves tested on 0.7 to 10 m<sup>3</sup> vessels with 100 to 800 mm pipes. This study considers the simple configuration of a flap valve connected to a vented vessel-straight duct arrangement. The explosion in the vessel triggers the closure of the initially opened flap valve and should be effective within a short delay to prevent the flame from passing. The explosion in the vessel drives both the fluid flow in the pipes and the flap valve closing duration. The sudden closing of the pipe induces a complex fluid flow, including significant pressure and velocity fluctuations around the flap valve and a backflow towards the vessel. The commonly used empirical laws, such as those displayed in the EN standards on dust explosions, do not account for these fluid-structure interactions. A hybrid code has been developed to describe the fluid flow throughout the assembly. This code combines an integral model for the vessel and flap explosions, a 1D Eulerian method relying on a MacCormack scheme for the pipes, and a damped pendulum model for the flap solved using an RK4 scheme. The model results compare satisfyingly well with experimental results. The discussion focuses on analysing the problem's physics, from which design engineering rules are derived.

### 1. Introduction

When it comes to industries that handle combustible dust, pipelines are often utilised to connect different equipment, vessels and silos. When the risk of dust explosions is identified, more than prevention measures may be needed, and protective measures become necessary. Explosion protection is the focus of several national and international documents that lay out functions, intended uses and dimensioning rules for specific systems. However, despite a few examples mentioned in the guidelines, most are limited to the description of protection applied to a single isolated piece of equipment, which is different in industrial processes. Therefore, the recommendations provided in the guidelines can only be applied to an industrial site with careful consideration. A dust explosion occurring in one piece of equipment can spread flames and pressure to other parts of the plant. Moreover, there is a strong correlation between an explosion and its surroundings, and its effects may be considerably enhanced due to pre-compression and jet flame ignition in interconnected enclosures. Explosion Isolation is a critical component of a

comprehensive safety concept.

Although explosion vents are the most commonly used explosion protection techniques on enclosures that may undergo a dust explosion, passive actuation flap valves are the most widespread pipeline isolation systems in the process industries. During regular operation, the process flow in the pipeline keeps the flap valve open. However, when an explosion occurs in a piece of downstream equipment, the pipe flow is inverted, leading to the flap valve's closure. This prevents the spreading of the explosion and effectively stops the pressure and the flames from propagating any further. The standard EN 16447 (EN16447, 2014) outlines the general requirements for explosion isolation flap valves. However, like any standard, it can only provide general recommendations and specifications but not address every application in detail. As with any explosion mitigation device, passive isolation flap valves work only within well-defined conditions, and the physics at stake makes their design challenging, mainly because of their strong interaction with the reactive gas flow. For instance, the problem is implicit: determining the minimum installation distance depends on the time needed for the

\* Corresponding author.

E-mail address: [yann.gregoire@ineris.fr](mailto:yann.gregoire@ineris.fr) (Y. Grégoire).

<https://doi.org/10.1016/j.psep.2024.02.003>

Received 28 November 2023; Received in revised form 30 January 2024; Accepted 3 February 2024

Available online 6 February 2024

0957-5820/© 2024 French national institute for industrial environment and risks (Ineris). Published by Elsevier Ltd on behalf of Institution of Chemical Engineers. This is an open access article under the CC BY license (<http://creativecommons.org/licenses/by/4.0/>).

pressure waves to reach the flap, which can only be known if the distance between the vessel and the valve is known. Thus, there is a need for a model that is simple enough to be run extensively in a wide range of situations with a low computational cost and complex enough to account for the dominant behaviours observed during the explosion isolation.

Only passive isolation valves are considered in the current study. Although the devices can rely on a different design from one manufacturer to another (use of counterweight or springs, variable angular amplitude), practically all rely on the same general principle of an inclined flap in a cylindrical tunnel that is maintained open by the flow during regular operation and closed by the flow reversal in the event of an explosion (see Fig. 1.).

In 2005, Moore (Moore and Spring, 2005) conducted research on active barriers that use flame-inerting agents to prevent gas and dust explosion flames from spreading through ducts. He derived empirical laws that govern the propagation of these flames. However, unlike flap valves, the duration to achieve isolation with these active barriers is constant and independent of the explosion effects. A model describing the dynamics of the flap would be necessary to complete this theory.

In 2016, Sippel (Sippel et al., 2016) highlighted the reverse effects that a functioning flap valve may have on the vessel undergoing an explosion. When the flap closes, the flow is reversed towards the vessel, which can sometimes enhance combustion (). This phenomenon is problematic because it can lead to unexpected pressure effects that may exceed the pressure resistance of the nevertheless protected equipment.

Later, Grégoire (Grégoire, 2023) presented experimental methods, measurements, and findings, along with a description of the physics involved in the vessel, pipes, and flap valve. This model can determine the minimum installation distance for the flap valve but cannot describe the events that occur once the flap valve is closed, such as the backflow towards the vessel and the critical role played by the ducts located after the flap valve.

Alternatively, Boeck (Boeck et al., 2021) derived phenomenological laws for the flame trajectory and backpressure effect in a vented vessel-duct arrangement. However, the description of the flap dynamics needs to be included to obtain a complete modelling solution, as no flap-flow interaction is accounted for in this approach.

More recently, Farrell (Farrell et al., 2022) published experimental measurements and demonstrated an isolation failure mechanism due to the piping behind the flap valve. He showed that poor experimental procedures during the certification of certain flap valves carried out without a pipe behind the valve have led to the certification and marketing of systems incapable of fulfilling their function in their prescribed conditions.

The current paper proposes a hybrid method combining analytical, phenomenological and computational fluid dynamics (CFD) to model the flap valve behaviour in various configurations. The gas flow – flap valve interaction is also modelled, which was not in earlier studies. The

model developed is tested to verify its capabilities to represent the dominant experimental trends and to draw good practice rules for implementing flap valves in the process industries.

## 2. Reference experimental configuration

### 2.1. EN16447:2014 recommendations and alternative testing method

EN16447:2014 (EN16447, 2014) defines the functioning conditions of passive isolation flap valves and gives requirements on the flap valve testing procedures suitable for their certification.<sup>1</sup> The testing procedure is split over three modules, dedicated respectively to the flap resistance to the explosion overpressure, the flame isolation capabilities of the closed device and its function on a fan-equipped installation. The standard also specifies that within a set of flap valves, at least the larger and the smaller sizes must be tested, and their functioning limits must be investigated. A direct consequence is that several ATEX fans will more likely be needed to conduct the experiments on the set of flap valves, and they may be damaged in case of failure of the isolation device. Above the potentially extreme costs of such work, one can note some difficulties in generating reproducible dust clouds with known concentrations and turbulence levels in the pipes. Thus, to perform functional testing of the flap valves, a better-controlled testing procedure is presented hereafter.

### 2.2. Experimental analysis

As an alternative method, we suggest holding the flap open by an external mechanism and releasing it when reaching a certain threshold linked to the explosion in the vessel. The difficulty lies in setting the release conditions for the flap in each situation. For this reason, preliminary experiments were conducted using a fan to blow air through the valve and black powder in the vessel to produce a well-defined pressure pulse mimicking a dust explosion. The setup comprises a vented 1 m<sup>3</sup> explosion vessel, a 12 m long DN160 transparent pipe, a flap valve (at 6 m from the vessel) and a fan used in a "push flow" configuration (see Fig. 2).

An advantage of such a procedure is that it is unnecessary to maintain and control an explosive dust atmosphere in the whole assembly (which would also threaten the fan). The fan produces an airflow towards the vessel. Once a quasi-stationary velocity is reached in the pipes (around 25 m/s), a pack of black powder from 50 g to 175 g is ignited in the 1 m<sup>3</sup> vessel. The latter is equipped with a DN80 side vent (in addition to the DN160 pipe) to limit the explosion overpressure within the 150 to 700 mbar range. This pressure is close to that obtained with an ST2 dust explosion in the vented vessel (see Fig. 3). The vessel overpressure leads to an inversion of the gas flow in the pipes and triggers the flap valve.

In Fig. 3, one of the signals has been shifted in time to highlight the similarity of both measurements regarding pressure rise rates. Despite the black powder explosion generating a longer impulse, the growth rate of the vessel pressure and the maximal amplitude are very similar to those obtained with a dust explosion. It can be concluded that the flow reversal dynamics induced by the explosion in the pipe remain similar in both cases.

The starting time of the flap valve closing and the closing duration were measured using image processing techniques to detect the change of directions of the air/smoke flow near the flap, together with pressure signals analysis before and behind the flap. While the instant closing of the duct can be measured with satisfying accuracy from the pressure profiles around the flap, determining the flap departure time is more challenging. The detection algorithm relies on a synthetic Schlieren method that we developed (Grégoire, 2014). Its accuracy is on the order of 1–3 images for the stopping time of the flap and 5–10 images for the departure time. Most tests were carried out with acquisition rates of

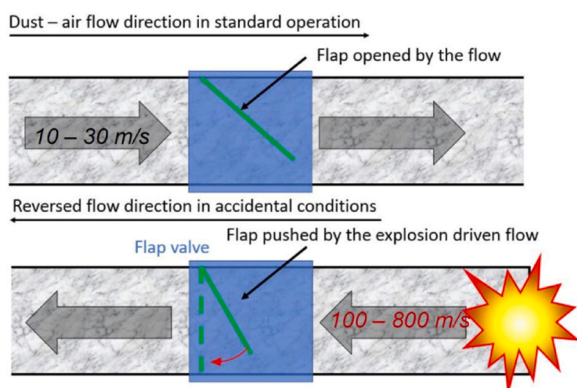


Fig. 1. Functioning of a passive flap valve.

<sup>1</sup> Note that this standard is under revision when writing the current paper

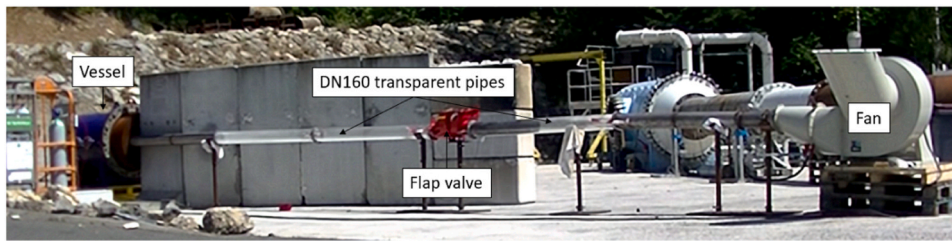


Fig. 2. Simulation of dust explosion isolation tests in a DN160 duct with a flap valve, using a fan and black powder in a 1 m<sup>3</sup> vessel.

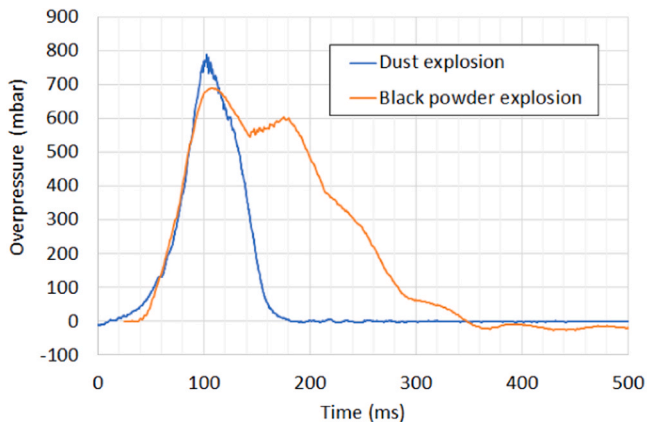


Fig. 3. Overpressure signal measurements during explosions in a vented 1 m<sup>3</sup> vessel performed with 175 g of black powder or 500 g/m<sup>3</sup> of wood cellulose dust ( $K_{St}$  measured in the same vessel of 230 bar.m/s). To aid comparison, the black powder signal was offset by 25 ms.

4000 images per second, leading to uncertainties on these measurements below a millisecond for the flap arrival time and less than 3 ms for its departure.

The image processing also allows the measurement of the flow velocity in the transparent ducts before and after the flap but not inside it. Such information is relevant as it can be compared to the departure time of the flap. With a sufficient rate of acquisition (typically above 1000 frames per second: the setup is a few meters long, and the explosion typically lasts for a few hundred milliseconds with flames and gases travelling at 100–500 m/s), it is possible to track features such as a flame front or moving dust agglomerates in a transparent pipe. In the present case, the dust naturally present in the device is sufficient to track the flow velocity in the pipe. We assume that the velocity of particles travelling in the transparent duct is the same as that of the carrying gas. An example is provided further in this paper (in Section 4.2) on a more illustrative experiment (in the presence of combustible dust and a propagating flame).

The other sensors on the duct (pressure gauges) are also used to estimate the flow velocity. The application of the Bernoulli formula between the two pressure sensors located right before and after the flap leads to a velocity of the airflow of 10 to 30 m/s at the flap's departure time (the tested valve was instrumented so that the pressure is measured at not more than 15 cm from each side of the closed flap). Note that it corresponds to pressure differences of about 50 to 600 Pa, measured on pressure sensors that measure up to 100 kPa overpressures. Thus, the accuracy of such measurement could be better in addition to the fact that the flap induces poorly known head losses that vary with the transient flow velocity. The cross-section inside the open flap is not that of a straight duct. For these reasons, the measurements were also confronted with numerical modelling with the code described further in the paper.

These works concluded that the flap, initially held open by the fan-induced airflow, only starts moving once the airflow has been compensated at the flap location by the counter-flow induced by the

explosion in the vessel.

### 2.3. Alternative method for functional testing of flap valves

These works allowed us to propose our reference configuration for the functional testing of passive isolation flap valves. This reference configuration is that of a vented vessel connected to a straight pipe arrangement along which the tested flap valve is mounted. An example is shown in Fig. 4.

An explosive dust atmosphere is generated so that the cloud can fill the whole volume (vessel and ducts). When necessary (above 4 m of a pipe diameter more prominent than 300 mm), an additional injection of dust is added to the pipes to fill the experimental device with an explosive atmosphere. In such cases, secondary dust injection devices are placed on the pipes, consisting of pressurised air-particle bottles connected to a perforated steel pipe in the ducts used for the testing. They create a combustible atmosphere along the entire length of the experimental setup. In any case, calibration tests were performed to ensure the combustible atmosphere was present when the flame entered the pipes and allowed its propagation over the entire length of the pipe.

After the dust ignition in the vessel, the flame expands and propagates in the duct. However, the flap valve is maintained open by an external device until the flow velocity due to the explosion exceeds a threshold velocity (typically 30 m/s) representative of the valve's intended use. Once this velocity threshold is reached, the flap is released and starts closing “freely”. In practice, we calibrated an electro-magnet piloted by a flow velocity measurement located a few meters ahead of the flap valve, with an actuation threshold set based on the measured flow velocity and the mechanical and electrical delays of the device. Deeper details on the sensor used to measure the velocity in the pipes were published by Proust (Proust and Jamois, 2021). Once released, the flap is submitted to the gravity force, and the explosion accelerates flow in the duct, the latter being, in our tests, the dominant effect. To achieve better observation control, transparent ducts are used on a small scale, with up to DN300 for pipes, as shown in Fig. 4. At larger scales (DN800), windowed pipes are used close to the flap valve.

The events are recorded by a high-speed camera at 2000 to 6000 frames per second. An indicator is systematically added to the valves tested to measure the flap opening angle as a function of time. Pressure is measured in the dust injection bottle ( $P_b$ ), in the vessel ( $P_v$ ), right before ( $P_{f1}$ ) and after ( $P_{f2}$ ) the flap valve (following the explosion direction, the flap valve itself is instrumented with the pressure sensors). This study tested fine wood cellulose dust with  $K_{St}$  at about 250 bar.m/s.

Compared to the test configurations proposed in EN16447:2014 (EN16447, 2014), there is no fan and no initial dust-air flow in the vessel-pipe assembly. The flap valve must also be held open until a specifically chosen time. Thus, the calibration procedure of the experimental setup can be more demanding. However, this setup offers better flexibility and control of the experiments. The combustible atmosphere is better controlled with this alternative approach, not only in the pipes but also in the test vessel where the explosions are ignited.



- 1 m<sup>3</sup> ISO vessel, 8 m of transparent ducts (PMMA), DN300 valve, + 2 m of ducts after the valve
- 700 g/m<sup>3</sup> of cornstarch dust (KST = 200 bar,m/s ; Pmax = 9 bar)
- Ignition with 2 x 5 kJ igniter at the duct entrance
- DN450 vent (aluminum foil, opens at 250 mbar)

Fig. 4. Image of the test setup for a DN300 flap valve located at 8 m from the explosion vessel. The flap valve is hidden due to confidentiality reasons. Pv, Pf1 and Pf2 indicate the positions of the pressure sensors.

#### 2.4. The course of events during explosion isolation

This paragraph gives a short description of the events that we intend to model. Deeper information on the experiments was provided by Grégoire (Grégoire et al., 2019). Passive flap valves were tested on 0.7 to 10 m<sup>3</sup> vessels with pipes of 100 to 800 mm diameter. As described in the earlier paragraph, the configuration of a flap valve connected to a vented vessel-straight duct arrangement is considered. An explosive dust cloud is generated in the assembly and ignited in the vessel. The initially opened flap valve is triggered by the explosion in the vessel and must close within a delay short enough to prevent the flame from passing. Before the valve closes, the explosion accelerates the flow, and large velocities can be reached in the duct (typically 200 m/s with a vented vessel, but as much as 800 m/s is possible with no vents). Upon valve closing, the flow's kinetic energy is converted into heat and pressure in front of the valve (on the explosion side). At the same time, a depressurisation is observed behind it (on the isolated side). Typically, a factor 4 between the pressure in the vessel and the pressure measured at the valve can be observed. Then oscillations appear on both sides of the flap and may lead to flame breakthrough. Experiments also demonstrate that the pressurised gases in front of the closed flap valve induce a backflow towards the vessel, which may lead to significant combustion enhancement and overpressure in the vessel. The parametric experimental study performed in the scope of certification of the tested flap valves aims to investigate the limits of the devices and their possible installation distances from the vessel. The numerical modelling of the experiments described afterwards aims to reach a satisfying understanding of the underlying physics so that design rules can be drawn for the intermediate and not-tested configurations.

### 3. Numerical description

#### 3.1. General description

A schematic description of the model is presented here to ease the reading of the subsequent parts. Note that all this code was implemented in Python, specifically for flap valve function modelling. The code is also provided within a Zenodo repository at the address <https://doi.org/10.5281/zenodo.10160617>, Grégoire (2023). Both an executable version and the source of the code are provided for research and educational use. The dimensions listed in the calculation input files are fictional due to confidentiality reasons related to the tested products.

Three main components are part of the study: the vented vessel, the pipes, and the flap valve. Three different approaches are used simultaneously for those three components. The reference situation of the modelling consists of the following:

- An explosion vessel, protected by a vent, connected to the pipe that needs to be isolated. The vessel may have another permanently open area.
- The first portion of the pipe in which the explosion needs to be isolated, referred to as Pipe1
- The flap valve is described as follows:
  - o Two connected vessels (i.e., two confined explosion models next to each other, the same as that used for the main vessel) are referred to as the flap body and the protected zone.
  - o A door between both vessels initially opened, then closed following a damped pendulum model solved with a 4th-order Runge Kutta scheme.
- The second portion of the pipe where the explosion needs to be isolated is Pipe2.

In both pipes, the gas flow is described by Euler equations, solved with a MacCormack scheme (MacCormack, 1969) with artificial viscosity. Suppose it is intended to model the presence of a fan in a push or pull flow situation. In that case, the code allows the setting of a driving pressure at the vessel side (also setting a dimension for a permanently open area to model a pull flow situation) or at the far end of Pipe2 (for a push flow situation).

A schematic summarising the models' architecture is provided in Fig. 5.

It is certainly not the first time a dust explosion in a vessel-duct arrangement has been modelled using CFD, given sizing a mitigation solution. However, the number of published works on this topic is scarce. Vingerhoets (Vingerhoets et al., 2013) published 3D CFD calculations on dust explosion propagation from a vessel to two pipes. A significant difficulty in modelling the vessel's initial explosion was highlighted, not to mention the absence of a functioning flap valve in this approach due to the code limitations. Sippel (Sippel et al., 2016) also performed 3D CFD calculations on similar configurations without a duct in the protected zone. In Sippel's approach, the flap closure is modelled as a more straightforward time-dependent function based on an empirical approach, and its dynamics are not correlated with the gas flow in the pipe. Using a 1D modelling offers the advantage of performing "hybrid" calculations, mixing CFD with a phenomenological description of the explosion in the vessel and an analytical pendulum model for the flap valve. More recently, Boeck (Boeck et al., 2021) proposed an alternative approach based on more straightforward physical considerations through a phenomenological approach, thus not relying on a CFD computation. Despite the clear advantages of such a method, in terms of ease of understanding and calculation costs, the capabilities of the code are limited to the prediction of the vessel over-pressure and flame trajectory in the pipe, quite independently from the flap valve behaviour. In practice, as shown later in the current study, the dynamics of flap closing are strongly affected by the flow in the

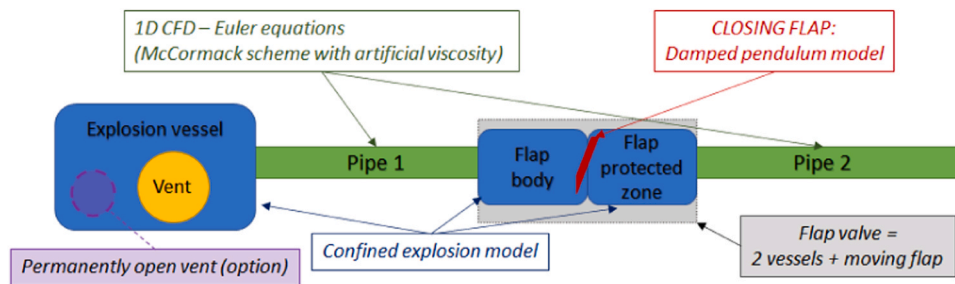


Fig. 5. Schematic of the code architecture.

pipes, and vice versa.

### 3.2. The vented vessel

The typical situation is a flammable cloud of suspended particles in a partially confined space: the vented vessel. The size, composition, and internal level of turbulence depend on the injection system and the geometric characteristics of the vessel. When the ignition source is triggered (with 2.5 kJ chemical igniters in the present case), the cloud ignites, and a flame propagates step by step from the ignition point. The flame develops spherically around the ignition source. On its way, it almost instantaneously converts cold reactants into hot combustion products (typically from 1000 to 2000 °C). Hot gases are less dense than cold ones, resulting in a high-volume gas expansion. This process is directly responsible for increasing the pressure in the enclosure. The rise in pressure due to the dust explosion is directly linked to the competition between the gases produced by the combustion and the gases lost by the various openings on the vessel (ducts, opened vents). Thus, the pressure rise curve as a function of time can be estimated with a model such as that of Lewis and Von Elbe (Lewis and von Elbe, 1987):

$$\frac{1}{P} \frac{dP}{dt} = \gamma \cdot \frac{Q_{\text{produced}} - Q_{\text{lost}}}{V} \quad (1)$$

$P$ ,  $V$  and  $\gamma$  are the enclosure pressure, volume, and the specific heat ratio of the gaseous species.  $Q_{\text{produced}}$  and  $Q_{\text{lost}}$  are the volumetric fluxes produced by the combustion and lost through the vent. This model indicates that the effect of the explosion will be directly linked to the reacting products, which will determine the gas production rate and the environment through the action of the vents and other openings in the  $Q_{\text{lost}}$  parameter. Note that the chemical reaction takes the simplest form of reactants becoming burnt products through a thin flame front (no flame thickness), and only one value of  $\gamma = 1.4$  is considered for both mediums. The combustible atmosphere has the same density as air ( $1.2 \text{ kg/m}^3$ ) at a 101325 Pa pressure.

To allow better flexibility in the modelling, the code permits setting a positive or negative fan overpressure. In the first case, the border condition at the extremity of Pipe 2 is set to model a blower fan using its pressure. In the second case, the negative overpressure is set at the permanently open flange on the vessel to model a suction fan. Both cases allow the modelling of push-flow or pull-flow situations as defined in EN16447:2014 (EN16447, 2014). An ignition delay must be set to establish a quasi-stationary flow in the vessel-duct assembly. Another option is to start calculations with an increased vessel pressure and specify an ignition delay to model the dust injection in our experiments.

#### 3.2.1. Gas production term

Estimating the gas flux  $Q_{\text{produced}}$  relies on the reactivity of flammable dust and the geometric arrangement that will influence the flame surface or promote concentration and turbulence gradients. The excess volume produced per unit of time is proportional: on the surface of the flame, the combustion rate of reactant consumed per unit of flame surface (this parameter has the dimension of a speed and is often called "burning rate"), and the volume expansion ratio (linked to the temperature of the

products: the hotter, the more volume is produced). Gas production through combustion can be approximated as follows in our model: the fresh combustible mixture is instantaneously transformed into hot burnt products through the passage of the flame whose thickness is zero. Thus, it is a function of the area of the reacting surface  $A_f$ , its velocity  $St$  and an expansion ratio  $E$ :

$$Q_{\text{produced}} = St \cdot A_f \cdot (E - 1) \quad (2)$$

Firstly, the expansion ratio  $E$  is thermodynamic data which depends only on the heat released by the combustion and can be expressed through the first principle of thermodynamics:

$$E = \frac{\rho_{\text{fresh}}}{\rho_{\text{burnt}}} \approx \frac{T_{\text{burnt}}}{T_{\text{fresh}}} = \frac{\Delta H_{\text{Comb}}}{C_p \cdot T_{\text{fresh}}} + 1 \quad (3)$$

With  $\Delta H_{\text{Comb}}$ , the reaction enthalpy  $T_{\text{fresh}}$  and  $T_{\text{burnt}}$ , the temperatures of the reactants and the burnt products,  $\rho_{\text{fresh}}$  and  $\rho_{\text{burnt}}$  the densities of the reactants and the burnt gases, and  $C_p$  the specific heat of the burnt products. The expansion ratio  $E$  is a fundamental parameter that depends strongly on the composition of the combustible mixture and is poorly influenced by flame propagation. It varies between 4 and 8 for the most common mixtures found in the process industries (Proust, 2017). Alternatively, the shape of the confined structure suffering the explosion can influence the flame surface  $A_f$ , and so is the case for the local flow velocities or when obstacles are present. The flame grows spherically in a medium at rest until the spherical front reaches the closest wall. When contacting the wall, the flame front is stopped and then reversed. During this phase, the flame front surface can become cellular or be curved toward the combustion products. The maximal flame area is linked to the dimensions of the volume and its cross-section. Extensive comparisons of INERIS code EFFEX calculations (Proust, 2005) that rely on similar equations with experiments indicate that a decent agreement can be achieved when the maximum flame surface is roughly equivalent to the largest inscribed hemisphere in the enclosure (Proust, 1999). Before this, a hemispherical growth is assumed (as most tests are ignited close to the wall of the vessel).

Finally, the flame velocity in a mixture attached referential is also expected to be a property intrinsic to the mixture. The fundamental combustion velocity  $S_{\text{lad}}$  obeys the laws of thermokinetics (thermodynamic equilibrium, Arrhenius law). It can be described as the volume of reactants consumed by a square meter of the flame area. However, this definition corresponds to a configuration in which the reactive mixture is at rest, in which case the effect of an explosion would be limited. A more realistic approach consists of relying on the turbulent flame velocity  $St$ .  $St$  can be considered a constant proportional to  $K_{\text{St}}$  in a first approximation. Even in the isolated enclosure, the effects of the dust explosion are strongly dependent not only on the nature of the reactants but also on the specificities of their environment, such as the geometry or local turbulence effect. The current study sets  $St$  empirically based on the tests performed without the flap valve.

The vessel fluids are split between a fresh and a burnt phase to determine the explosion duration. At each time step, the expansion of the burnt products induces an isentropic compression of the fresh

mixture. Then, the flame consumes a certain amount of reactants (proportionally to the flame surface  $Af$  and velocity  $St$ ). At the same time, another portion escapes (or enters) through the vent or in the pipe (proportionally to the sections concerned and the pressure difference).

### 3.2.2. Gas loss term

$Q_{lost}$  can be estimated through various models derived from the generalised Bernoulli's laws. In practice, whether the flow is subsonic or supersonic, it is possible to estimate the  $Q_{lost}$  term through Eqs. (4) or (5), respectively, for the subsonic and supersonic cases:

$$Q_{lost} = C_d \cdot S \cdot \left(\frac{P_2}{P_1}\right)^{1/\gamma} \cdot \sqrt{\frac{2 \cdot \gamma}{\gamma - 1} \cdot \frac{P_1}{\rho_1} \cdot \left(1 - \left(\frac{P_2}{P_1}\right)^{\frac{\gamma - 1}{\gamma}}\right)} \quad (4)$$

$$Q_{lost} = C_d \cdot S \cdot \sqrt{\gamma \cdot \frac{P_1}{\rho_1} \cdot \left(\frac{2}{\gamma + 1}\right)^{\frac{\gamma + 1}{\gamma - 1}}} \quad (5)$$

In the code, depending on the flame position relative to the open area, fresh gases, burnt gases, or a combination of both may be ejected through the vent. In practice, a spatial flame velocity is computed based on a linear composition of the flow velocity at the flame front, based on the initial reactive consumption rate ( $St$ ) and the burnt product expansion rate ( $E$ ), with the terminal flow velocity at the opening  $Q_{lost}/S$ . Shortly, if the base velocity (computed from  $St$  and  $E$ ) is  $V_1$  and the gas velocity at a vent is  $V_2$ , then the spatial flame velocity at a distance  $x$  from the ignition point, towards the vent at a distance  $L$  from the ignition point is calculated as  $V_{flame} = V_1 \cdot x/L + V_2 \cdot (1 - x/L)$ . Once the flame has reached a vent (or opening to a pipe), fresh and burnt gases are ejected with respect to their volume fraction in the enclosure:  $V_U/(V_U + V_B)$  for the reactants and  $V_B/(V_U + V_B)$  for the burnt products.

The model described in the previous paragraphs is only applicable if the flame propagation velocity is sufficiently low (typically  $< 30$  m/s) for the internal pressure to remain "uniform". This condition is generally satisfied when the ratio between the largest and smallest dimensions of the apparatus is less than 5 (Proust, 1999), which is not the case for pipes, for example.

## 3.3. The pipes

### 3.3.1. Governing equations

The biphasic nature of the fluid flow is not accounted for in this model; only an ideal compressible fluid is considered. Also, the fluid dynamics in the pipe are modelled using the compressible Euler equations in their conservative form. Such a choice was made as the sudden closure of the flap sometimes leads to the emission of shockwaves in the pipe. Furthermore, our interest in industrial safety is more focused on assessing conservative estimations of the observed events. The Navier-Stokes equations set would have been more relevant if we intended to describe the combustion reaction in the pipe, which is not the case here. The flame front is considered an interface that instantly transforms the fresh reactants to burnt products at a combustion rate  $St$  equal to that used in the vessel.

As we intend to model the progressive closure of the flap valve in the pipe, it is necessary to examine the pipe section as a function of time and the evolution of the gas dynamics during the flame propagation and the valve's closure. A quasi-one-dimensional transient compressible model using Euler formalism was judged sufficient for this. As a result, the equation system, also including an equation of state (ideal gas) linking the pressure and the internal energy, for the pipes is:

$$\left\{ \begin{array}{l} \frac{\partial A \cdot \rho}{\partial t} + \frac{\partial(\rho \cdot u \cdot A)}{\partial x} = 0 \\ \frac{\partial(A \cdot \rho \cdot u)}{\partial t} + \frac{\partial(\rho \cdot u^2 \cdot A)}{\partial x} + A \cdot \frac{\partial P}{\partial x} = 0 \\ \frac{\partial A \cdot E}{\partial t} + \frac{\partial[(E + P) \cdot u \cdot A]}{\partial x} = A \cdot Q \\ \frac{\partial A \cdot \rho \cdot Y_u}{\partial t} + \frac{\partial(\rho \cdot u \cdot A \cdot Y_u)}{\partial x} = A \cdot \omega \\ P = (\gamma - 1) \cdot \left(E - \frac{\rho \cdot u^2}{2}\right) \end{array} \right. \quad (6)$$

With  $t$  the time,  $x$  the abscissa,  $A$  the pipe section,  $\rho$  the fluid density,  $u$  the longitudinal velocity,  $P$  the pressure,  $E$  the energy,  $\omega$  the species consumption rate,  $Q$  the heat production,  $\gamma$  the specific heat ratio. This Q1D CFD model was inspired by rocket nozzle modelling, which was the basis for its initial development. It was intended to model a duct with a locally reduced cross-section at the flap location, progressively closing. The first intention was to split the pipe into two sections separated by a closed wall as soon as the valve was closed entirely. Unfortunately, this solution was lacking stability. When the flap body is large compared to the duct section (by a factor of 2 in some of our experiments with the smaller flap valves), the steep cross-section variation led to unphysical shocks travelling back to the vessel before any flap movement. Furthermore, it was also unsuited to account for possible secondary explosions in the flap valve body.

As a result, it has been decided to rely on a purely 1D description, using two pipes: one before the flap and the other after it. Both are treated the same way, with the same resolution scheme. Only the boundary conditions differ. Thus, equation set 6 (Eq. 6) is simplified to:

$$\left\{ \begin{array}{l} \frac{\partial \rho}{\partial t} + \frac{\partial(\rho \cdot u)}{\partial x} = 0 \\ \frac{\partial(\rho \cdot u)}{\partial t} + \frac{\partial(\rho \cdot u^2)}{\partial x} = 0 \\ \frac{\partial E}{\partial t} + \frac{\partial[(E + P) \cdot u]}{\partial x} = Q \\ \frac{\partial(\rho \cdot Y_u)}{\partial t} + \frac{\partial(\rho \cdot u \cdot Y_u)}{\partial x} = \omega \\ P = (\gamma - 1) \cdot \left(E - \frac{\rho \cdot u^2}{2}\right) \end{array} \right. \quad (7)$$

In our approach, the heat production term  $Q$  is set to 0, but it is still present in the code (so it can be implemented later).

### 3.3.2. Resolution

The resolution of the equation system (Eq. 7) is based on a MacCormack method. This method was chosen because of its satisfying accuracy, low computational cost, and robustness for subsonic and choked flows. For a given equation in the form of:

$$\frac{\partial V}{\partial t} + \frac{\partial(W)}{\partial x} = S \quad (8)$$

MacCormack's method relies on a 2 step fluxes predictor-corrector model. Firstly, the prediction step starts with estimating an intermediate field denoted  $\overline{V}_i^{n+1}$  corresponding to a preliminary value of the field  $V$  in cell  $i$  at the time step  $n + 1$ . Because in our configurations, we may encounter subsonic and choked regimes, damping unphysical perturbations and adding a numerical viscosity term is often necessary. For each field  $V$ , this dissipation term takes the form:

$$D_V = C_x \cdot \frac{|P_{i+1}^n - 2 \cdot P_i^n + P_{i-1}^n|}{P_{i+1}^n + 2 \cdot P_i^n + P_{i-1}^n} \cdot (V_{i+1}^n - 2 \cdot V_i^n + V_{i-1}^n) \quad (9)$$

with  $P$  the local pressure and  $C_x$  a coefficient set by the user. Further details on this approach may be found in Anderson's book (Anderson, 1984). Then, the predicted value for field  $V$  is:

$$\overline{V_i^{n+1}} = V_i^n - \frac{\Delta t}{\Delta x} \bullet (W_{i+1}^n - W_i^n) + \Delta t \bullet S_i^n + D_V \tag{10}$$

When relevant, the predicted terms  $V_i^{n+1}$  are then used to update the fluxes terms  $W_{i+1}^n$  and  $W_i^n$  to  $\overline{W_{i+1}^n}$  and  $\overline{W_i^n}$  and the source term  $S_i^n$  to  $\overline{S_i^n}$ . New diffusion terms  $\overline{D_V}$  are also built similarly but using the "predicted" pressure rather than the initial one. The predicted pressure is obtained with the last equation in equation set (Eq. 7) from all the other "predicted" fields:

$$\overline{P} = (\gamma - 1) \bullet (\overline{E} - 0.5 \bullet \overline{p} \bullet \overline{u} \bullet \overline{u}) \tag{11}$$

Finally, the corrector step is:

$$V_i^{n+1} = \frac{1}{2} \bullet (\overline{V_i^{n+1}} + V_i^n) - \frac{1}{2} \bullet \frac{\Delta t}{\Delta x} \bullet (\overline{W_{i+1}^n} - \overline{W_i^n}) + \frac{\Delta t}{2} \bullet \overline{S_i^n} + \overline{D_V} \tag{12}$$

### 3.3.3. Combustion in the pipe

No gas production due to flame passing is considered in the current model. Earlier experiments and phenomenological analysis (Grégoire, 2019) indicated that for the organic dust considered (of  $K_{St}$  lower than 250 bar.m/s), at the scale considered (up to 10 m<sup>3</sup> with 15 m of DN800 ducts), there were no significant effects of the combustion in the duct. This may not remain true with metal dust or at larger scales. If needed, the effect of the dust combustion could be added, including a heat source term. In practice, in the conditions considered in this study, it has been observed that the flow in the duct entirely drives the flame propagation in the duct. In the current model, only the flame position is calculated, based on the assumption of a 1-cell long flame front with the same velocity as the gas in this cell. The flame starts in the vessel at the ignition location. It expands following the phenomenological approach used to model the confined explosion in the vessel. It eventually enters the pipe. Then, the flame trajectory is constructed from assembling the successive positions taken by the flame front in the duct. A function is, however, left empty in the code, in which any user can implement a heat production model.

### 3.3.4. Border conditions in the pipe

Three locations need to be addressed:

- the connection between the vessel and the pipe
- the exit of the pipe
- the varying conditions at the flap valve (initially opened, then entirely closed)

The flap valve is modelled as two connected yet separate enclosures to avoid the complex definition of a border condition that would vary with the pipe cross-section in the vicinity of the flap. On one side, the flap body is modelled as an explosion vessel, open towards a "protected zone", which is also an explosion vessel of diameter and length  $D$ , the pipe diameter. Further description of the flap valve is given in paragraph 3.4. Thanks to this formulation, all border conditions may be treated the same way in the pipes. The number of border conditions that need to be specified at each extremity of each pipe varies depending on the flow regime. Shortly, one must differentiate inflows, outflows, and choked and subsonic regimes. With an entering choked flow, all variables (density, momentum, energy) must be set. The supersonic outflow is independent of the outer atmosphere (in practice, the value in the border cell is the same as in the cell next to it). In the subsonic regime, only the pressure is specified for the outflow (the other parameters are interpolated from the inside of the pipe). In contrast, the pressure and density are specified for the inflow case. These rules are summarised in

Table 1:

Table 1 Border conditions in the pipes.	
	Supersonic
Inflow	Density, momentum, and energy are specified by the driving vessel or flap.
Outflow	Density, momentum and energy are the same as in the adjacent cell.
	Subsonic
Inflow	Pressure and density are specified from the driving vessel / flap / atmosphere. Momentum is interpolated from the state within the pipe. Energy is computed from Eq. (11).
Outflow	Pressure is specified from the downstream condition. Density and momentum are interpolated from the state within the pipe. Energy is computed from Eq. (11).

There is still a weakness in this formulation due to the simplifications made with the 1D geometry. At the second pipe extremity, in the atmosphere, low-density burnt products (around  $0.2 \text{ kg/m}^3$ ) are ejected (in case of failed isolation or absence of the flap). A compression wave from the outer atmosphere will eventually come back towards the vessel, and keeping the external air density at 1.2 will lead to the generation of an artificial discontinuity and possible failure of the calculation. This is not a significant issue as, at this stage, the result of the calculation is already known. To avoid this situation, it is assumed that the gas density coming back from the outside is 95% of the gas already at the border of the pipe and 5% of air ( $P = 1.01325 \text{ bar}$ ;  $\rho = 1.2 \text{ kg/m}^3$ ). This numerical artefact does not impact the results and is used only when there is no flap or an isolation failure. However, it helps maintain calculations for the duration specified by the user.

### 3.3.5. Time steps and mesh sensitivity

The spatially discretised variables are vectors because the calculation is performed over a single dimension. Python language was selected to implement the model because it is an interpreted programming language in which all variables can be accessed during the calculation and supports vectorisation. Thus, the code is reasonably readable, robust, and able to handle hundreds of thousands of time steps over thousands of cells within a few minutes. Because the computational cost is low enough, only limited analysis was performed on mesh sensitivity and an oversized discretisation was systematically chosen. In most cases investigated, the cell resolution was on the order of a few cm (for 5 to 20 m long pipes), and the Courant number ( $CFL = u \cdot dt/dx$ , with  $u$  the velocity,  $dt$  the time step and  $dx$  the mesh size) was set from 0.15 to 0.25. Also, an artificial viscosity coefficient is set in the input data, and values ranging between 0 and 0.8 were tested successfully. Larger values for this dissipation coefficient slow the fluid flow to a limited extent. As an order of magnitude, on a tested case of a  $1 \text{ m}^3$  vessel with 8 m of pipes, the larger value of the dissipation coefficient (0.8) delayed the flap characteristic functioning times by 1 ms over 60 ms of total closing duration and the final flame position in the duct by 10 cm. These discrepancies remain reasonable at this scale, and it is believed that deeper investigation would be needed for other scales.

### 3.4. The flap valve

The flap valve testing was first performed in the absence of any explosion to measure the flap closing delay when submitted only to the gravity force. Those tests showed that independently from the flap valve supplier, the trajectory of the inner flap can be well predicted with a simple model of a damped pendulum, which takes the form:

$$\ddot{\theta} = -m_v \cdot l_v \cdot \frac{g}{J_\Delta} \cdot \sin(\theta - \theta_i) \quad (13)$$

with  $m_v$  the mobile parts mass (kg),  $l_v$  the distance between the axis and their barycentre,  $k$  a damping factor,  $J_\Delta$  the moment of inertia, and  $\theta$  the flap angle with the vertical axis. Performing a test without the explosion allows the empirical determination of the  $k$  coefficient for a given flap valve. In practice, the flap is released, and its free fall is monitored with a high-speed camera. The other dimensional parameters being easily accessible, measuring the flap angle as a function of time allows the determination of the value of  $k$  in Eq. (13). A comparison of such model performance with an experimental result is shown in Fig. 6:

Then, when an exploding dust-air flow is pushed on the valve, the closing delay is reduced. It can be quite satisfyingly calculated by adding a pressure force contribution to the earlier equation:

$$\ddot{\theta} = -m_v \cdot l_v \cdot \frac{g}{J_\Delta} \cdot \sin(\theta - \theta_i) - \frac{k}{J_\Delta} \cdot \dot{\theta} - \frac{\Delta P_c \cdot l_v}{J_\Delta} \cdot S_v \cdot \cos\theta \quad (14)$$

with  $P_f$ , the pressure force applied on the valve depends on the pressure difference between both sides of the flap and the dynamic pressure effect

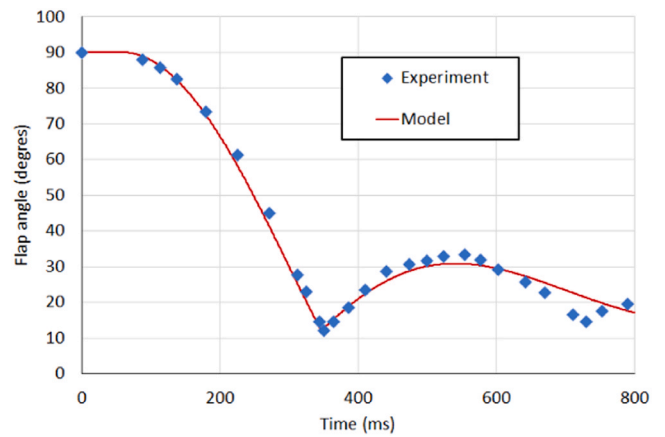


Fig. 6. Model fitting over an experiment of free-fall closing of a flap valve to determine the damping coefficient  $k$ .

of the particle-laden flow on the flap. It is interesting to point out some specificities of this model. First, concerning the numerator, the inertial term  $m_v \cdot l_v \cdot g$  will more likely range around  $1\text{--}500 \text{ kg} \cdot \text{m}^2 \cdot \text{s}^{-2}$  if we assume masses in the 1 to 50 kg range for flaps between a DN100 and a DN1000. Alternatively, on the pressure term  $\Delta P_c \cdot l_v \cdot S_v$ , assuming a 100 mbar overpressure leads to a range of 10 to 10000  $\text{kg} \cdot \text{m}^2 \cdot \text{s}^{-2}$  for the same devices. This points out a dominance of the pressure effect over the flap inertia, consistent with experimental findings: typically, a flap closing freely (only under the effect of gravity) within 300 ms may be shut within 50 ms when submitted to an explosion pressure. Secondly, the denominator in formula (Eq. 14) is the inertia momentum of the moving flap. It implies that heavy, thus more resistant explosion-proof designed elements will start moving slower than light (and more fragile) elements of lower inertia. Thus, when developing such a device, because end users want it to be as fast as possible (to reduce the minimum installation distance) but strong enough to withstand the explosion, the flap valve producers would target a low inertia flap with a high-pressure / shock / impact resistance. Improvements may also be made to the friction of the device or the total angle that needs to be covered during the closing of the flap (the lower, the better).

### 3.5. Back to the vented vessel

When an explosion occurs in a structure of interconnected enclosures, the typical industrial case, it can be transmitted from one vessel to its neighbours, and the flame propagation can become highly complex (Phylaktou et al., 1999). In such case, a schematic of a possible course of events is presented in Fig. 7: the dust ignition in the primary enclosure induces a first explosion (Fig. 7a). It generates significant turbulence and flow velocity in the connected pipe (Fig. 7b). Then large quantities of the combustible mixture will be pushed in the downstream enclosure and pressurise it. After its significant acceleration in the duct, the flame will enter the pressurised and highly turbulent combustible mixture in the secondary volume. A secondary explosion of much greater violence can then happen (Fig. 7c). It can also reverse the flow completely and push the reactive front back into the primary vessel where the combustion is not terminated (Fig. 7d), thus enhancing it. Experiments show similar behaviour when the second enclosure is a flap valve.

In such an event, the situation is that of Fig. 7b, where the duct is "suddenly" closed (i.e., at maximum within a few tens of milliseconds, from our experience with such devices). Similar to Fig. 7c, a counter-pressure is generated downstream of the duct, i.e., at the valve, leading to a flow reversal towards the vessel. Thus, the turbulence level in the vessel is enhanced, and the first estimation made earlier on the St parameter may not be valid anymore. A direct consequence can be a secondary pressure rise in the vessel, as shown on the right side of Fig. 7.

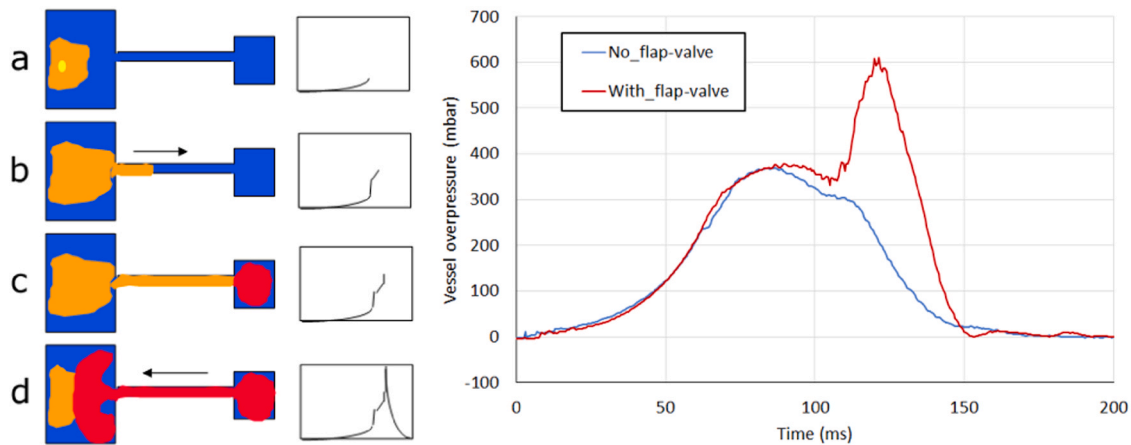


Fig. 7. Schematic representation of explosion development in interconnected enclosures and example of experimental measurements on a 1 m<sup>3</sup> vessel with a DN160 flap valve located at 5 m.

Its existence has also been shown experimentally by Sippel (Sippel et al., 2016) and Grégoire (Grégoire et al., 2019). This secondary pressure rise may be problematic in certain occurrences as it is not accounted for in most models and not even mentioned in the European standard EN 16447:2014 (EN16447, 2014) used for the certification of such isolation valves (which is, however, anterior to those published results, and currently under revision). In other words, it is necessary to correct the rate of consumption of the reactants in the vessel whenever a backflow from the flap occurs.

An option has been added to model this phenomenon: it has been decided to consider that the gas flow rates coming back to the vessel will proportionally increase the flame velocity. The backflow of burnt gases enters the vessel with a flow rate  $Q_{\text{back}}$  over the pipe cross-section. It is chosen to conserve this flow rate and distribute it over the vessel cross-section  $S_{\text{vessel}}$  to obtain a volumetrically averaged flow velocity that is added to  $St$ :

$$St_{\text{modified}} = St + Q_{\text{back}} / S_{\text{vessel}} \quad (15)$$

This approximate model introduces an average flow velocity term in calculating the flame velocity. The objective is to describe a turbulent flame "carried" by the flow from the pipe. The tank's geometry and the vent's position should impact this flow velocity so that it is difficult to measure without resorting to complex tools, such as determining an induced turbulence field in the vessel.

#### 4. Results and discussion

Results of the computations are presented based on a test in which a DN160 flap valve was placed on a transparent duct at 4.5 m from the standard ISO6428 1 m<sup>3</sup> vessel vented with a DN300 plastic foil holding up to 350 mbar. An additional 2 m long transparent pipe is positioned after the flap valve. The combustible dust consists of 500 g of wood

cellulose. It is placed in a 20-bar pressurised bottle of 5 litres. Ignition is performed 450 ms after dust injection starts with  $2 \times 5$  kJ chemical igniters located in the vessel and close to the pipe inlet in the present example (note that the standard specifies that central and back ignition should also be investigated). The vent opens when the overpressure reaches 350 mbar in the vessel. An image captured during this test is presented in the following picture (Fig. 8). The flap is hidden due to confidentiality reasons:

The hybrid CFD-integral model is run, and the results are compared with several experimental records: the vessel overpressure ( $P_{\text{red}}$ ), the pressure records before ( $P_{\text{fl}}$ ) and after ( $P_{\text{fl}}$ ) the flap valve, the flame trajectory extracted from the high-speed camera records as well as the position of the indicator needle of the side of the flap valve (which is directly linked to the flap).

##### 4.1. Pressure records

In the vessel, the integral model efficiently describes the early steps of the explosion, with a first pressure rise and then a change in the slope when the vent opens, around 350 mbar in the present experiment (Fig. 9):

The subsequent evolutions are due to the interaction with the pipe flow and, more precisely, to the flap closed at  $t = 85$  ms after ignition. The model prediction fits satisfyingly with the experimental data despite a slight discrepancy in the signal shape and the maximum overpressure due to secondary compression and enhanced combustion effects.

The records before (on the vessel, unprotected side) and after the flap (on the protected side) also agree reasonably well with the experiment (Fig. 10.a, Fig. 10.b, Fig. 10.c.), especially in terms of frequencies of the signals:

Before the flap valve closes, both signals follow the same trend. However, when the flap closes:

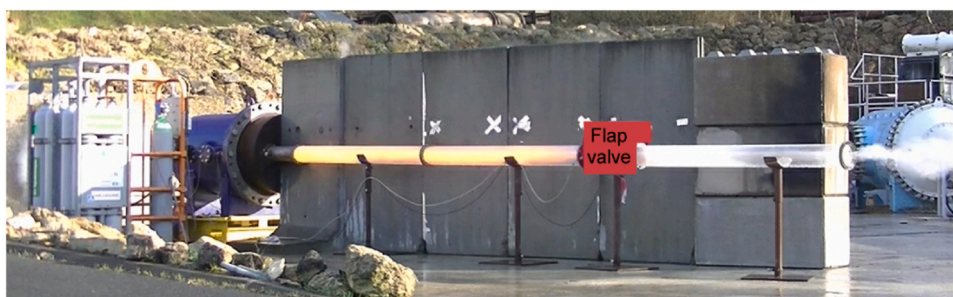


Fig. 8. Image of the example test captured by the HD camera.

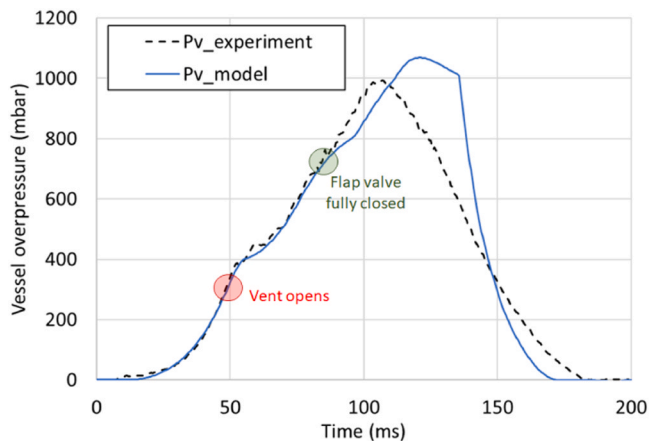


Fig. 9. : Vessel overpressure – Experiment vs. Calculation.

- on the unprotected side (the vessel side), the pressure rises due to the deceleration and then the stopping of the gas column in front of the flap. The pressure in front of the flap eventually becomes more significant than that in the vessel, leading to an inversion of the gas flow and, later, oscillations.
- On the protected side, the gases move away from the closed flap, generating a vacuum and, thus, a depression. The model reproduces this effect very well. However, when the depression wave reaches the end of the pipe, a compression wave is emitted back to the flap, and oscillations ensue.

The trends and amplitudes are globally respected despite the more considerable overestimation of the pressure level on the unprotected side when the flap closes in the present example. This difference is likely due to the simplified description of the flap body, assumed to be a straight cylinder in this approach. Earlier experiments with the Quasi-1D model (Eq. 6) and a more precise description of the flap body led to better estimations (yet lower robustness of the calculations). Secondary oscillations are of significant amplitude because no viscous nor inertial damping has been added to the model. We remind that it is developed in the scope of industrial safety, thus aiming to assess the maximum effects of an explosion on the industrial process. Accounting for the heat of combustion in the first pipe would also help better estimate the oscillation frequency in that part of the system. Inaccuracies may also arise from a lack of modelling of the actual biphasic flow in the equation of state selected in the model. Here, the energy absorption from the particle acceleration is not considered, leading to a more conservative estimation of the overpressures. This seems acceptable for the present purpose of understanding the interaction between the flap valve and the flow and helping to define the functional limits of this isolation device. In particular, the presence of a duct after the flap, which is representative of most industrial applications, implies negative overpressures at the moment of flap closing because of the sudden stopping condition imposed ahead of the moving gas flow. Once the rarefaction wave reaches the end of the pipe, a compression wave returns towards the flap (highest pressure peak in Fig. 10.b). The unsynchronous oscillations between the front and the back of the flap valve may lead to situations where the pressure after the flap is higher than in front of it (see the negative part in Fig. 10.c). In such a case, it has been observed experimentally, especially with the larger flap valves, that these oscillations may break the flap locking mechanism and re-open the flap valve, thus allowing flame transmission. This underlines the need to test/model flap behaviour in the presence of a pipe after the flap valve. Also, on this specific aspect, the acoustic imperfection of the model, which does not dampen the oscillations, helps identify these potentially critical situations.

## 4.2. Cinematographic records

It is possible to extract the flame trajectory as a function of time. To do so, an  $x-t$  diagram of the flame trajectory is constructed by selecting a straight line on the original video as a reference (for instance, the line located on the axis of the pipe). This selected reference line of pixels is extracted from each video frame, and the whole is superposed vertically in chronological order from bottom to top to form a new image. The typical result of such an operation is shown in Fig. 11:

The pressure oscillations depicted in Fig. 10 at the origin of the visible particle density and flame position oscillations in this  $x-t$  diagram. In the present example, the light grey area is the particle cloud. It looks darker in low-density areas because the white powder reflects the sunlight. From an image such as Fig. 11, it is possible to extract the successive positions of the flame front and compare those with the model predictions (Fig. 12, left). Also, locating manually on some of the frames of the video the position of the angle of the flap allows us to compare its position to that modelled in the code (Fig. 12, right):

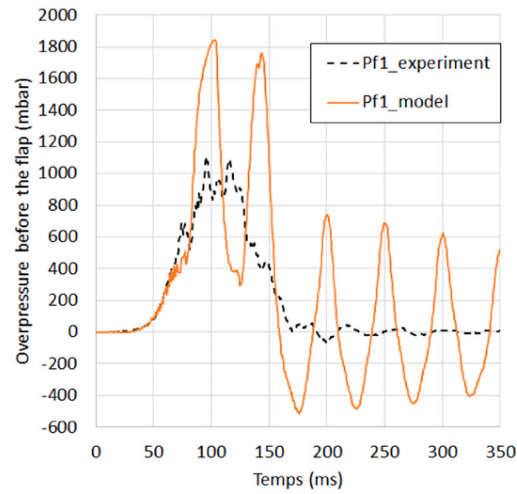
The agreement is acceptable in both cases despite a few differences in the initial acceleration of the flap valve. The transparent pipe section is set up to 4.6 m from the vessel in the current case. The flap closes at 5.1 m from the vessel, which explains the earlier stopping of the flame in the experimental case in Fig. 12. (It is not stopped at 4.6 m but is hidden and not visible after this point).

## 4.3. Other experimental findings and how the code complies with the physics of the problem

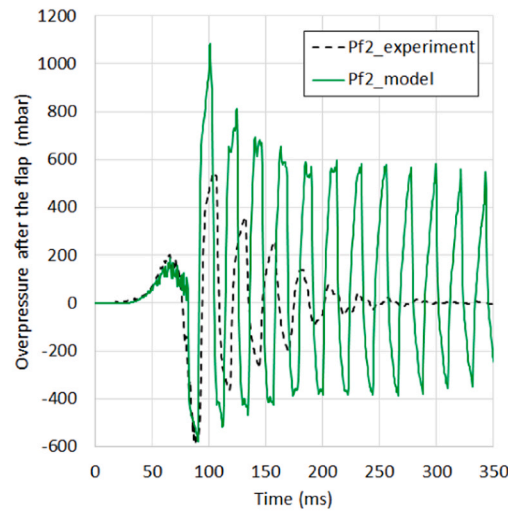
### 4.3.1. The role of the downstream pipe

This model has been successfully confronted to experiments with flap valves from DN100 to DN800 in explosion vessels of volumes of 0.4, 0.7, 1 and 10 m<sup>3</sup>, the larger flap valves being tested in the larger vessel and vice-versa. Both experiments and calculations highlight the critical role of the downstream pipe in the protected zone after the flap valve. The explosion in the vessel drives the fluid flow in the connected pipes. Around the flap valve, the fluid pressure or velocity plays a dominant role in its closing duration. At the instant of the complete closing of the duct, the fluid velocity near the flap drops to zero, and the conservation Eq. (7) induce a pressure rise on the unprotected side of the flap and a vacuum on the protected side. Schematically, the sudden stopping of the flow is transformed into pressure as in a hammer struck. At the same time, the reverse phenomena are observed downstream of the closed flap, inducing a large underpressure pulse. This evolves to oscillations (in pressure, velocity, and density) on both sides of the flap that may lead to its re-opening or destruction (refer to Fig. 10). On the vessel side, the burnt gases of lesser density (as compared to the fresh reactants) will more easily lead to higher frequency oscillations, which may be of lower amplitude (when it is primarily an inertial effect). In opposition, on the protected side of the flap valve, in case of successful isolation, the denser fresh reactants with lower sound speed will lead to lower frequency oscillations of possibly larger amplitude. This can happen when the events are dominated by inertial effects without significant energy release from the combustion. Indeed, the oscillations' amplitude on the vessel side also depends on the combustion, so a "lower amplitude" is not granted. Then, it eventually leads to a higher pressure after the flap valve than before, which can break its locking mechanism and re-open the flap valve. This is mainly observed on large flap valves (DN400 and above). Farrell (Farrell et al., 2022) performed experiments on different (certified) flap valves available on the U.S. market. He also pointed out this failure mechanism.

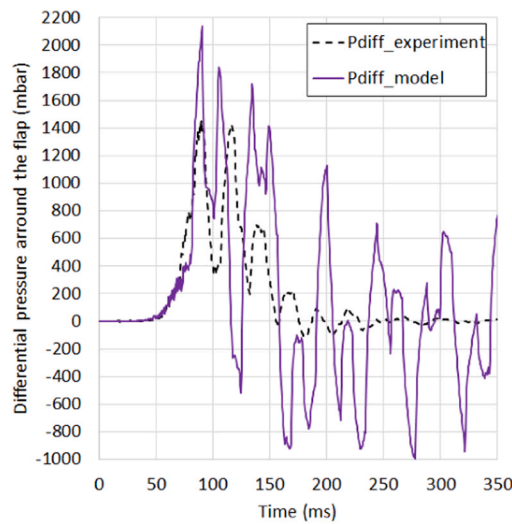
In the model, thanks to the excellent agreement in the frequencies of the downstream oscillations with the experiments, it is also possible to investigate the conditions of occurrence of such phenomenon numerically. In the absence of a duct on the protected side, which is not representative of the industrial configuration in which the flap valve is to be used, there are no comparable efforts applied to the back of the flap



**a:** Pressure before the flap – Experiment vs. Calculation



**b:** Pressure after the flap – Experiment vs. Calculation



**c:** Pressure difference around the flap – Experiment vs. Calculation

**Fig. 10.** **a:** Pressure before the flap – Experiment vs. Calculation. **b:** Pressure after the flap – Experiment vs. Calculation. **c:** Pressure difference around the flap – Experiment vs. Calculation.

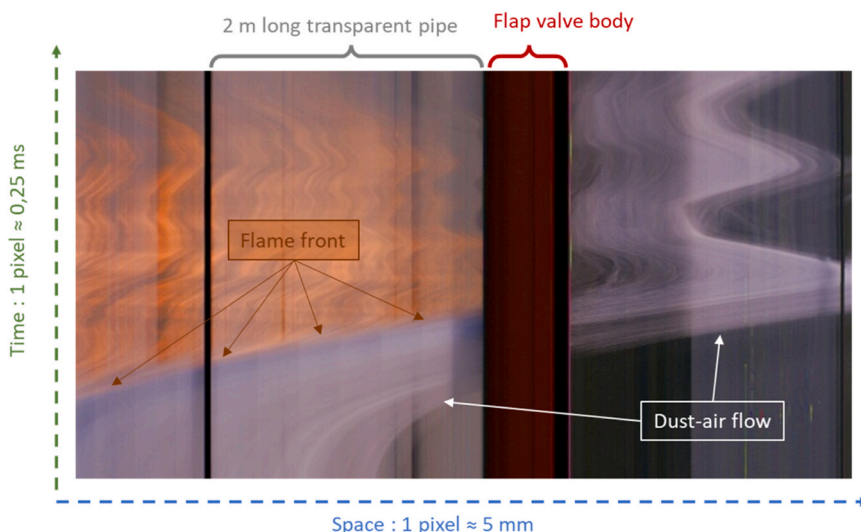


Fig. 11. Video extracted x-t diagram showing the flame trajectory. Vertical superposition: position is in abscissa and time in ordinates. The reddish band around the centre of the picture is the flap valve.

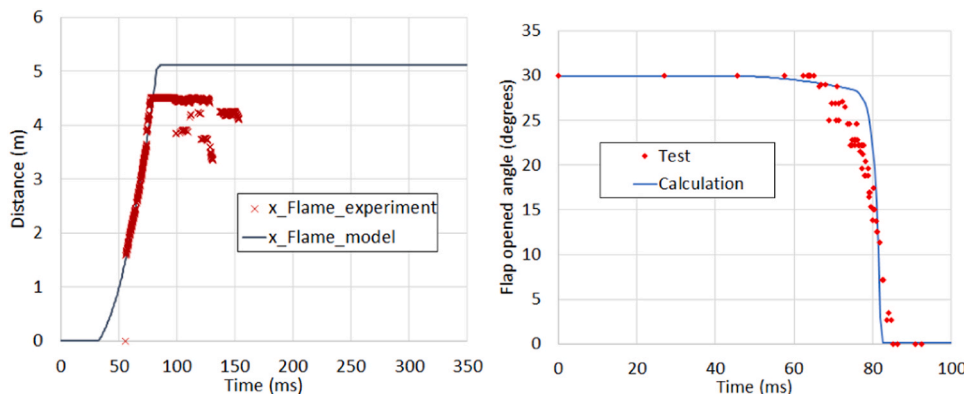


Fig. 12. Flame front trajectory(left) and flap opening angle as a function of time (right)– Experiment vs. Calculation.

valve. A significant change in the current revision of the EN16447 guideline is not only a mandatory duct length after the flap in the testing procedure of such devices but also the introduction of a need to investigate unfavourable coupling conditions of the gas flow around the flap valve.

4.3.2. Enhanced combustion in the vessel due to the backflow from the closed flap

Also, calculations show that the sudden closing of the flap valve induces a backflow towards the vessel that can be significant enough to increase the vessel pressure by a few dozen mbar under certain conditions: with the smaller vessels, vents and when the pipe is large enough compared to the vessel. Secondary explosion mechanisms in the vessel are mentioned in paragraph 3.5. As an illustration, experimental records from tests on a 0.7 m<sup>3</sup> vessel with a DN100 duct (with and without a DN100 flap valve located at 4 m from the vessel) are compared with calculations (with a flap valve) in Fig. 13.

As described in paragraph 3.5, the secondary explosion model is approximate. Its objective is to describe a turbulent flame "carried" by the flow from the pipe. As explained, the tank's geometry and the vent's position should impact this flow velocity. In the present case, it is assumed that the velocity of the reverse flow is entirely added to the consumption rate of the reactants. This is expected to be a conservative approach, and the over-estimation of the secondary pressure peak is a logical consequence.

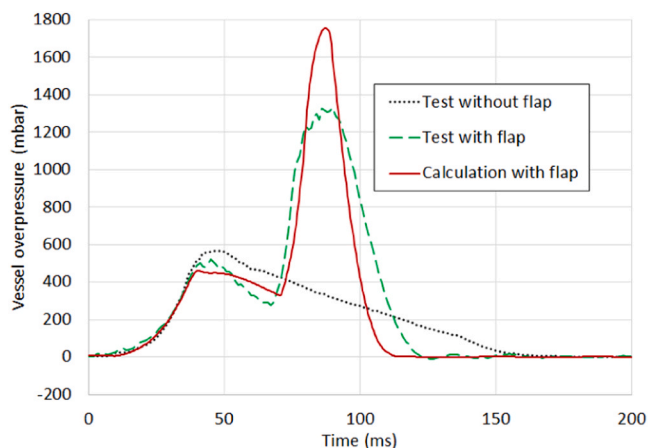


Fig. 13. Illustration of the backflow effect on the vessel combustion enhancement: wood cellulose explosion in a 0.7 m<sup>3</sup> vessel with a DN100 duct, with and without a DN100 flap valve located at 4 m on the straight pipe – Experiment vs. Calculation.

4.3.3. Identifying the characteristic functioning times of the whole vessel-pipe-flap valve assembly

The simplified combustion models added for the secondary explosion

in the flap (assuming a flame velocity identical to that in the vessel) and for the backflow-induced enhanced combustion in the vessel rely on rough approximations. As such, they tend to lead to over-conservative estimations. This result was expected, and it does not matter as it does not affect the flap valve's functioning times (the code's main result) and provides estimations on the safe side. The code allows us to switch on or off these models, temporise those effects and investigate their consequences. For example, in the case of a cornstarch dust explosion in a  $10\text{ m}^3$  vented vessel connected to a DN800 duct, the following pressure signals were measured (Fig. 14):

Before 175 ms, both pressure signals superpose relatively well, indicating a satisfying reproducibility of the experiments. However, beyond this point, secondary pressure bumps are seen in the case of the isolated duct. Running calculations while switching the various combustion options in the flap valve or the vessel allows the identification of the origin of these secondary evolutions (Fig. 15):

In this example, as described earlier, accounting for secondary explosions in the model leads to overestimating the overpressure in the vessel and front of the flap valve. However, the timing of these secondary evolutions is of more relevant interest in the present case: the calculation fits better, in terms of frequencies, with the experiment when it is assumed that the backflow from the flap leads to an enhancement of the combustion in the vessel. Alternatively, the calculation indicates that no secondary combustion in the flap valve body is needed to reach the pressure levels measured experimentally. Both in the test and the calculation, the flame reached the flap valve at  $t = 160\text{ ms}$ . The first dominant effect is losing a discharge area at the flap. It leads to increased overpressure in front of the flap valve and reverses the gas flow in the pipe. The second effect is the addition of compressed gases in the vessel. Then, the third effect would be an enhancement of the vessel combustion. Finally, the fourth effect is the pipe acoustics with compression waves travelling again towards the flap valve.

After  $t = 220\text{ ms}$ , both calculations diverge again from the experimental result: the pressure drops in the calculation while it is maintained in the experiment. As it did not exist in the flap valve experiment, this phenomenon could be due to the confined combustion in the duct. The present code is, however, unable to describe eventual heat production due to combustion in the pipe. Thus, investigating the maximum installation distance of a given flap valve is not directly possible. To do so, the user must implement a heat production model in the dedicated section of the code.

Computations can also be used more extensively to verify the

behaviour of the model in comparison to expected events. It is possible to model push-flow and pull-flow configurations when a fan-induced flow is present in the pipes, which fits better with the industrial application. Examples of these configurations are given with the code in the input data CSV file. Note that for confidentiality reasons, only fictional dimensions were given in these examples; the objective is purely illustrative.

#### 4.3.4. Towards a better practice

As of today, the minimum and maximum installation distances for a given flap valve are tight to their commercial use. A small minimum installation distance indicates a fast-acting valve that can be placed closer to the equipment at the explosion's origin. This presents an advantage in space-constrained industrial processes. However, it should be kept in mind that the flap valve will not start closing before the explosion develops in the so-called equipment. If the flap valve can be placed near enough to the enclosure, it closes quickly, leading to a compression in front of the flap valve and a backflow that can enhance the primary combustion. Most frequently, such equipment is protected by explosion vents. In a vent-protected enclosure, the maximum overpressure is usually reached when burnt gases are ejected through the vent. If the backflow from the pipe arrives before this moment or while the vessel overpressure is still high, it is expected that the combustion can be significantly enhanced, potentially leading to overpressures larger than acceptable by the enclosure (then necessitating the addition of complementary mitigation solutions).

Alternatively, placing the flap valve farther on the duct allows for delaying the arrival of the backflow so that it can leave a negligible effect. The example input data provided with the code concerns a fictive DN200 flap valve on an 8 m pipe connected to a  $5\text{ m}^3$  vented vessel. In Fig. 16, the calculated vessel explosion overpressure signals are compared when the flap valve is placed at 4, 5 and 6 m from the vessel.

The model used in this approach may be over-conservative due to the simplifications made in their formulation. They can nonetheless represent characteristic variations on the pressure profiles that can be expected if the backflow from the flap valve arrives at an inopportune moment.

Secondly, the flap closing duration also plays an important role. In the earlier example (Fig. 16), the flap is the same for the three installation distances. If we now consider two other flap valves, installed at 5 m, in the same test conditions as in Fig. 16 but with a slower and a faster acting flap valve, we obtain the results of Fig. 17:

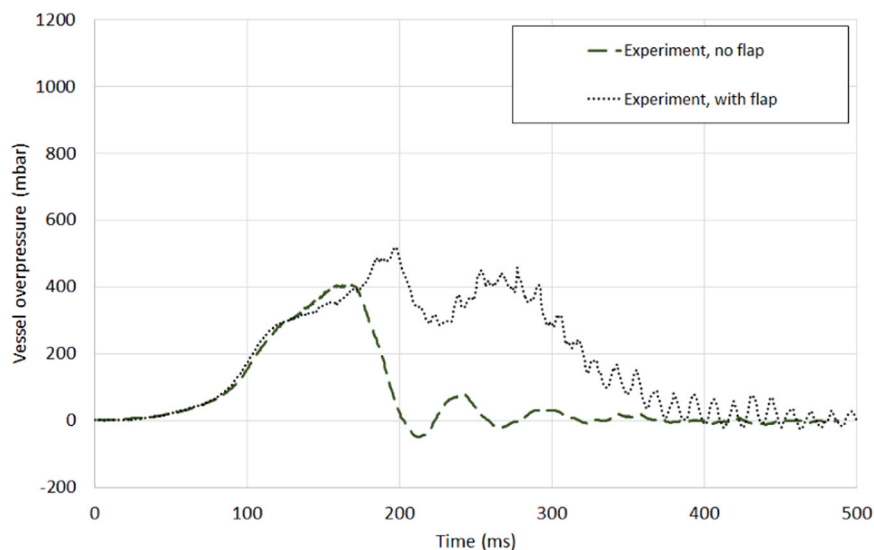


Fig. 14. Vessel overpressure during cornstarch explosions in a  $10\text{ m}^3$  vented vessel with a DN800 duct, with and without a DN800 flap valve located at 7 m on the straight pipe.

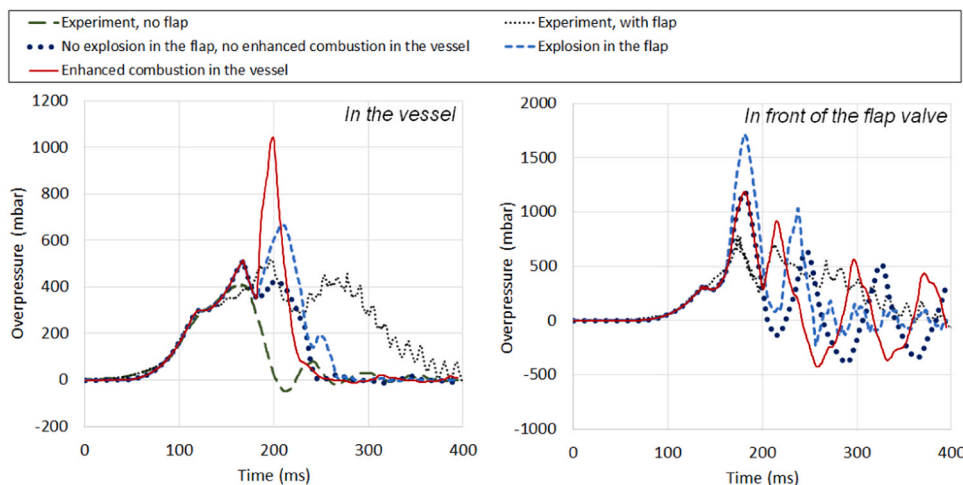


Fig. 15. Comparison of the experimental signals of Fig. 14 with calculation results assuming different hypotheses on the secondary combustion modelling.

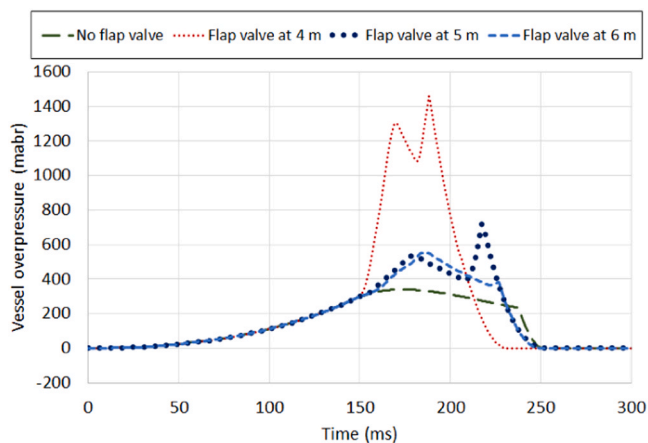


Fig. 16. Effect of the flap location on the induced overpressure in the vessel.

A slower-acting valve permits the flame to reach the flap valve body while gas pressurises it. A consequence is an intensified compression in the flap valve body and an increased backflow to the vessel. In the current example, the faster-acting flap valve closed while the flame was still 2 m away, while in the slower flap valve case, the flame entered the flap valve at the same instant. Thus, stopping the gas flow (closing the flap valve) while the flame is still far from the isolation device is better.

Finally, the maximum installation distance is usually related to the resistance of the flap valve. It is based on the conservative assumption that a flame propagating in a duct keeps accelerating, thus augmenting the associated overpressure, eventually past the flap valve resistance. In practice, in most cases, the vessel explosion is either vented or suppressed by dedicated mitigation systems so that past a specific time, the flame is not supported anymore by the vessel explosion. In our experience with organic ST1 dust, no significant flame acceleration was observed in ducts ranging from DN100 to DN800 with lengths up to 20 m. Compared to the tests performed at shorter distances, increased overpressure was sometimes overserved in front of the flap valve. However, they were due to inertial effects with the gas column deceleration when the flap valve closes and the flame's arrival in the pre-compressed gases in the flap body. The highest pressures were reached when the flap closed at the latest. This trend can be correctly

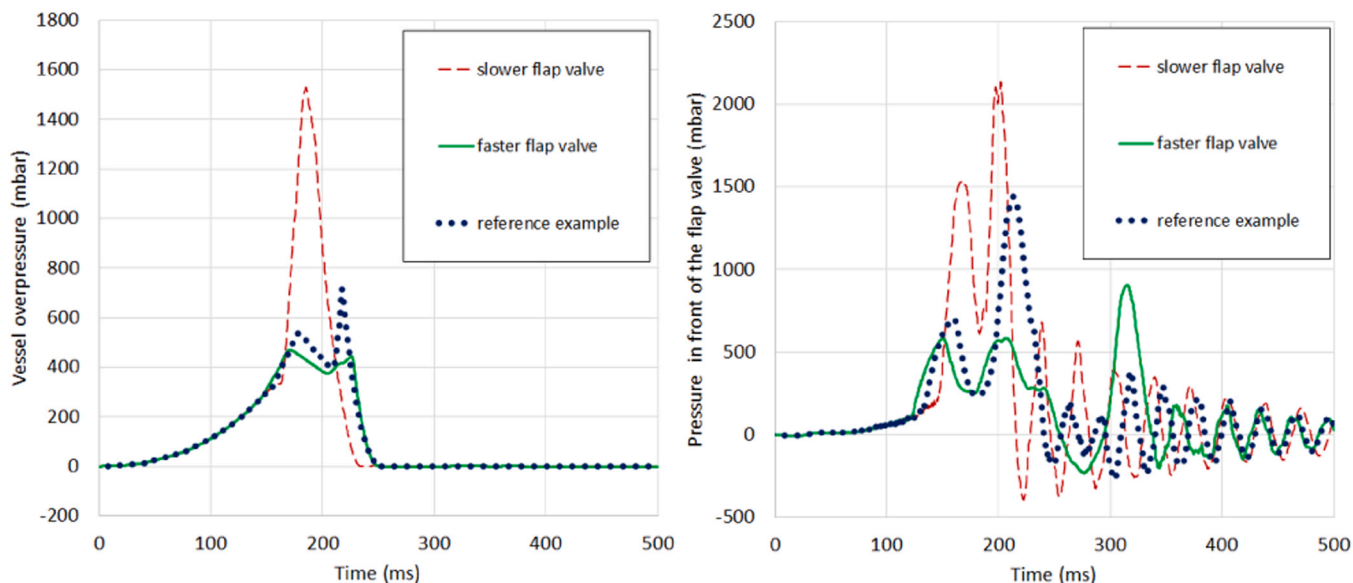


Fig. 17. Pressure signals in the vessel and front of the flap valve for three kinds of flap valves, all located 5 m from the example's 5 m<sup>3</sup> vessel.

modelled with the code. That is the main reason for the absence of a combustion model in the pipes in our model. With more reactive dust or larger scales for the duct assembly (in length or diameter), we infer that such a model would be needed.

Nonetheless, these works indicate that the worse pressure effects in the vessel would be obtained either with slower flap valves installed at their minimum installation distance or when the flap valve is at its maximum installation distance. There is a compromise to be found in between, where the backflow effect is more limited, and the possible pressure build-up due to combustion in the pipe is still acceptable.

#### 4.3.5. Potential and limitations of the model

The model proposed in the current study relies on a hybrid method combining analytical, phenomenological and computational fluid dynamics (CFD) approaches. It has been designed to be accessible and written in an interpreted language, allowing the user to control most of the variables while still being fast enough to perform computations on a standard computer within a few minutes. For example, it is possible to model push- or pull-flow situations, change the flap inclination or study the effect of various parameters such as the flap inertia.

The model is based on primarily conservative assumptions for the phenomenological modelling of the explosion, except for the combustion in the pipes, which is not calculated. The code still includes a function, presently returning 0, but that could be used to compute a heat generation or absorption in the pipes, provided the user completes it with a dedicated model.

It has been developed for a rough modelling of a generic valve. Several variables can be adjusted for a specific product to fit better with reality.

For the moment, the MacCormack scheme is a good compromise between the accuracy and performance of the calculations, but it could still be improved, for instance, by using a scheme with a TVD property. Also, our earlier tests with a Q1D formulation (Eq. 6) led to generally more accurate results. Such formulation could also be used to model the effect of local head losses. However, it was abandoned because it lacked robustness whenever there were significant size differences between the pipes and the flap body diameter. This effect could be mitigated using a different resolution scheme.

## 5. Conclusions

Passive explosion isolation flap valves were tested at Ineris. Because of the complex nature of the phenomena involved, including fluid-structure interactions, pressure, velocity oscillations, and enhanced vessel combustion events, simple tools appear limited to efficiently modelling the flap valve behaviour. However, because of the implicit nature of the problem and the multiplicity of solutions that may be encountered, it is necessary to rely on tools simple enough to perform the iterative calculation at an acceptable cost. For this reason, we developed a hybrid integral-CFD code. It relies on a phenomenological description of the explosion in the vessel, linked with a 1D modelling of the flow in the pipes. It is completed with a damped pendulum equation to model the interaction of the flap with the fluid flow. In light of easing the development and comprehension of the code, a single-time step was used for these three elements. A classical Euler time discretisation is used in the vessel, while the pendulum motion relies on an RK4 solver. The Euler equations for the flow in the pipes are solved using a MacCormack scheme. Improvements could be made in the equation of state to account for the biphasic nature of the gas-particle flow or the combustion model in the pipes. Only a perfect and inert gas is considered in the duct; it seems sufficient to cover our needs. A reactant consumption model is present in the pipes, but no combustion-induced heat is considered. The effect of pressure build-up due to dust combustion in the pipes is also not modelled for the moment, but the option to add a dedicated model is left free for the users. Also, despite the code offering the possibility to model vertically inclined flap valves, it is not directly

possible to account for the effect of bends or various head losses in the pipes. However, this could be improved by specifying localised heat, modifying the governing equation set (Eq. 7) or reverting to the initially proposed quasi1D formulation (Eq. 6). Whenever a backflow after the flap closing arrives in the vessel, an intensification of the combustion can be considered in the model. The model predictions compare satisfyingly well with experimental measurements. It is pointed out that the model allows the representation of experimental measurements, such as the gas flow oscillations before and after the flap valve or the impact of the latter's closing on the vessel overpressure. This is especially important as those two phenomena can directly be responsible for the critical failure of the mitigation strategy on an industrial process. In the first case, the oscillation may lead to the flap re-opening associated with a failure of the isolation. In contrast, in the second case, the safety of a complete process equipment may be corrupted.

### Declaration of Generative AI and AI-assisted technologies in the writing process

Statement: During the preparation of this work, the author(s) used Grammarly Business in order to check the spelling and grammar. After using this tool/service, the author(s) reviewed and edited the content as needed and take(s) full responsibility for the content of the publication.

### Declaration of Competing Interest

The authors declare that they have no known competing financial interests or personal relationships that could have appeared to influence the work reported in this paper.

## References

- Anderson, D.A., 1984. *Computational Fluid Mechanics and Heat Transfer*, 1984. Hemisphere Publishing Corporation, New York.
- Boeck, L.R., Bauwens, C.R., Dorofeev, S.B., 2021. Modeling of explosion dynamics in vessel-pipe systems to evaluate the performance of explosion isolation systems, 104477, ISSN 0950-4230 J. Loss Prev. Process Ind. Volume 71, 2021. <https://doi.org/10.1016/j.jlp.2021.104477>.
- EN16447:2014, Explosion Isolation Flap Valves, 2014.
- Farrell, T.M., Kakogiannis, D., Barfield, M., 2022. The wild west: quality control deficiencies in certification testing of explosion isolation flap valves. *American Institute of Chemical Engineers 2022. Spring Meeting and 18th Global Congress on Process Safety*.
- Grégoire, Y., Sturtzer, M.O., Khasainov, B.A., et al., 2014. Cinematographic investigations of the explosively driven dispersion and ignition of solid particles. *Shock Waves* 24 (2014), 393–402. <https://doi.org/10.1007/s00193-014-0500-0>.
- Grégoire, Y., Leprette, E., Proust, C., 2019. Function testing of passive explosion isolation flap valves. *Proceedings of the Ninth International Seminar on Fire and Explosion Hazards (ISFEH9. Saint-Petersburg, Russia*.
- Grégoire, Y. (2023). Passive isolation flap valve modelling tool. In *Process Safety and Environmental Protection* (1.0). Zenodo. <https://doi.org/10.5281/zenodo.10160617>.
- Lewis, B., von Elbe, G., 1987. *Combustion, flames and explosions of gases*. Acad. Press, Orlando.
- MacCormack, R.W. (1969). The effect of viscosity in hypervelocity impact cratering, *AIAA Paper*, 69–354.
- Moore, P.E., Spring, D.J., 2005. Design of explosion isolation barriers. *ISSN 0957-5820 Process Saf. Environ. Prot.* Volume 83 (Issue 2), 161–170. <https://doi.org/10.1205/psep.04231>.
- Phylaktou, H.N., Andrews, G.E., 1999. *Explosion development in pipeline systems and linked vessels UKELG 25th meeting. Ind. Combust. Hazards Jt. Meet. Combust. Inst. (Br. Sect. )*.
- Proust C. (1999). Prévoir les effets des explosions de poussières sur l'environnement, EFFEX, un outil de simulation. Available at [www.ineris.fr](http://www.ineris.fr).
- Proust, C., 2005. The usefulness of phenomenological tools to simulate the consequences of dust explosions: the experience of EFFEX. *International ESMG symposium. Nürnberg, Germany*.
- Proust, C., 2017. Turbulent flame propagation in large dust clouds. *J. Loss Prev. Process Ind.* 49, 859–869. <https://doi.org/10.1016/j.jlp.2017.05.011>.
- Proust, C., Jamois, D., 2021. Measuring the flow and the turbulence in a harsh environment using a modified Mc Caffrey gauge, 101993, ISSN 0955-5986 *Flow*.

Meas. Instrum. Volume 80, 2021. <https://doi.org/10.1016/j.flowmeasinst.2021.101993>.  
Sippel M., Schepp P., Hesener U. (2016). New Findings for the Application of Systems for Explosion Isolation with Explosion Venting Chemical Engineering Transactions Vol. 48, DOI:10.3303/CET1648089.

Vingerhoets J., Farrell T.M., Snoeys J., Dust Flame Propagation in Industrial Scale Pipelines - Part 2: CFD Study of a Conveying Vessel-Pipeline System, 9th Global Congress on Process Safety (GCPS), San Antonio, April 28 - May 1, 2013.